Interfacial Properties and Growth Dynamics of Semiconductor Interfaces

Phil Rosenow, Andreas Stegmüller, Lisa Pecher, and Ralf Tonner

Abstract We present computational results on dynamics and properties of semiconductor materials and interfaces. The adsorption of cyclooctyne on silicon can be shown to proceed barrierless into an *on-top* structure. Comparing different interfaces of the GaP/Si system, a preference for mixed interfaces (i.e. not purely Si/Ga or Si/P) can be found and understood in terms of the electrostatic potential across the interface and chemical bonding specifics. In further work, the electronic structure of mixed III/V semiconductors will be studied in the way described here for GaAs and used for the prediction of optical properties.

1 Introduction

The structure of interfaces and the dynamics of growth processes determine each other and the properties of the resulting material. Due to the importance of semiconductor devices for modern everyday technology, understanding the growth, structure and properties of semiconductor/semiconductor and semiconductor/organic interfaces will be decisive for the design of improved devices. Since these interface systems are generally complex, computational studies require a large amount of resources, especially when going beyond simple model systems toward descriptions of real materials.

Here, we present some examples of our recent work in this area. In Sect. 2, we show some results from a study shedding light on the adsorption of cyclooctyne on Si(001), which is a promising candidate for the functionalization of silicon with organic layers. Sections 3–5 evolve around III/V-semiconductors grown on silicon, a prospective material class for the construction of laser devices on silicon substrates: in Sect. 3, the composition of precursor molecules for gas phase epitaxy is described, which will be used as starting points for adsorption studies. In Sect. 4, the stability of various Si/GaP interfaces is described; Since this is often the first layer in a III/V

P. Rosenow • A. Stegmüller • L. Pecher • R. Tonner (✉)
Philipps-Universität Marburg, Fachbereich Chemie, Hans-Meerwein-Straße, 35032 Marburg, Germany
e-mail: rosenow4@staff.uni-marburg.de; stegmuea@Staff.Uni-Marburg.de; pecher@staff.uni-marburg.de; tonner@chemie.uni-marburg.de

© Springer International Publishing Switzerland 2016

W.E. Nagel et al. (eds.), *High Performance Computing in Science and Engineering '15*, DOI 10.1007/978-3-319-24633-8_13

laser structure, the interface has a strong influence on the properties of the final device. The electronic properties of the actual laser material will also be studied computationally, as is outlined in Sect. 5. Finally, we will present some data on the scaling behaviour of our main DFT code VASP on the Hornet cluster in Sect. 6.

2 Surface Reactivity of Cyclooctyne on Si(001) with DFT: Predicting Growth Processes for Semiconductor/Organic Interfaces

2.1 Introduction

Due to the strong binding character of their addition to the silicon(001) surface, [1, 2] cyclooctyne (Fig. 1) and its derivates promise to be ideal building blocks for the construction of semiconductor/organic interfaces. In order to predict the growth process leading to these interfaces, one has to understand the interaction between single molecules and the surface first. We gather this understanding by conducting density functional theory (DFT) calculations in a periodic environment and determine adsorption pathways of the molecule to the surface using the Nudged Elastic Band (NEB) method [3]. Afterwards, *ab-initio* molecular dynamics (AIMD) simulations are conducted to validate the previous results for finite temperatures. The experience gained here will later be transferred to the GaP/Si material system.

2.2 Computational Details

All calculations have been carried out with periodic DFT [4, 5] as implemented in the *Vienna Ab-initio Simulation Package* (VASP) [6, 7]. The chosen level of approximation was the Generalized Gradient Approximation (GGA) with the functional by Perdew, Becke and Enzerhof (PBE) [8, 9] and addition of the DFT-D3 (BJ) correction [10, 11] to account for dispersion interactions. The electronic structure was calculated in the projector-augmented wave (PAW) formalism [12, 13] using a plane wave cutoff of 400 eV. Due to the periodic boundary conditions, the silicon surface had to be treated in a slab approach (see Fig. 2) where a thickness of six layers of silicon was chosen with the bottom two layers being frozen and saturated by hydrogen atoms at 1.48 Å distance in the direction of the next bulk

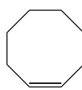

Fig. 1 Structural formula of cyclooctyne

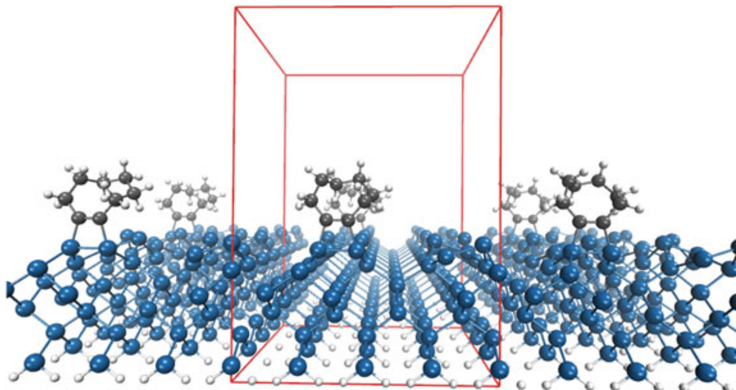

Fig. 2 Cyclooctyne bound to the Si(001) surface in the *on-top* configuration as an example for the slab approach in periodic boundary conditions, the *red box* highlighting the boundaries. Dimer formation due to surface reconstruction of the silicon atoms is also apparent in this figure

layer atoms to mimic the transition into the silicon bulk. The *on-top* reaction was calculated in a $c(4 \times 2)$ reconstructed cell with 48 silicon atoms in total, while for the *end-bridge* reaction and AIMD simulations the cell size was doubled along the short axis, leading to a (4×4) super cell with 96 silicon atoms. Reciprocal space was sampled using a Gamma-centered Monkhorst-Pack scheme, [14] where a $\Gamma(241)$ grid was used for the (4×2) cell while a $\Gamma(221)$ grid was used for the (4×4) cell.

Structural optimizations were done using the Conjugate gradient algorithm [15] while the NEB calculations utilized the limited-memory BFGS algorithm [16]. *Ab-initio* molecular dynamics simulations were done on the Born-Oppenheimer potential surface [17] with a timestep of $\Delta t = 1$ fs using a Verlet integrator [18, 19]. To account for finite temperatures, the Nosé-Hoover thermostat [20–22] was used within a *NVT* ensemble.

2.3 Optimizing Parallel Performance in VASP

Due to the high computational demand of NEB calculations and AIMD simulations, parallelization settings had to be optimized to values that enable the lowest possible cost of calculation time. The VASP code has several options for this, with the two parameters having the largest effect on computation time being KPAR and NPAR. KPAR enables the calculation at different k points at once while NPAR subdivides those groups to calculate different electronic states in the Self-Consistent Field (SCF) process in parallel. If, for example, one uses 64 cores with KPAR set to 2 and NPAR set to 4, the 64 cores are being split up into two groups of 32 cores each, who are working on two different k points simultaneously, while each of the two groups is again divided by 4, so in each subgroup, eight cores work on an individual

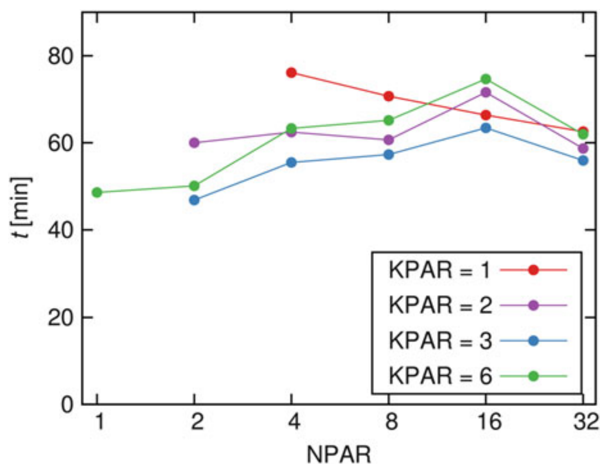

Fig. 3 Computation time of a single-point benchmark calculation in VASP as a function of the parallelization parameters NPAR and KPAR. Run on 192 cores on Cray XE6 (Hermit)

electronic state. For NEB calculations, several structures on the reaction path are being optimized at once, so a NEB calculation with 16 structures and equivalent performance to the example above would use $64 \times 16 = 1024$ cores.

To test the performance as a function of those two parameters, a benchmark single-point calculation in a (4×2) cell was set up on Cray XE6 (Hermit) using 192 cores, since most NEB calculations were done using 2048 or 4096 cores on 16 structures which corresponds to 128 or 256 cores working on a single structure. The results are shown in Fig. 3.

It can be seen that the best performance is achieved with NPAR = 2, KPAR = 3 and NPAR = 1, KPAR = 6, which both correspond to groups of 32 cores, exactly the amount of cores on one compute node. This tells us that minimizing inter-node communication is the most important factor in code performance optimization.

Subsequently, the chosen settings for the AIMD simulations, which were run on 1024 cores, were KPAR = 4 and NPAR = 8, so the cores were put in groups of 32 as well (the KPAR value arises from the larger cell size and corresponding smaller k mesh).

These setting should be well transferable to the Hornet machine with adjusting the values to the 24 core/node setting (see Sect. 6).

2.4 Nudged Elastic Band Results

There are two dominant ways in which the cyclooctyne molecule can bond to the Si(001) surface: In the *on-top* adsorption mode, a [2+2] cycloaddition takes place with two silicon atoms of a surface dimer, leading to a 4-ring structure of covalent bonds (see Fig. 2). In contrast to that, the *end-bridge* adsorption mode (Fig. 4) sees

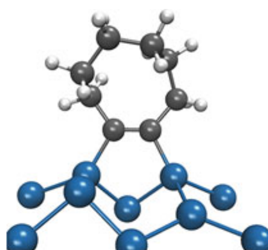

Fig. 4 The *end-bridge* adsorption mode of cyclooctyne bonding to the Si(001) surface, where the molecule reacts with two silicon dimers

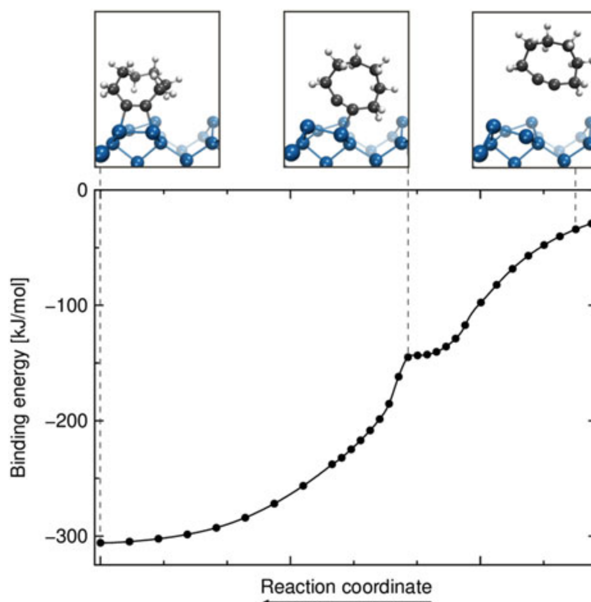

Fig. 5 Energy profile of the *on-top* adsorption path with structures shown at selected points. The binding energy is calculated with respect to the isolated and relaxed molecule and surface, respectively

the molecule bonding to one atom each of two neighbouring silicon dimers, leading to a 5-ring structure, and a change of 90° in the molecular orientation at the surface compared to the *on-top* mode. Over the course of both reactions, the C-C triple bond is being reduced to a double bond.

To find out which of the two adsorption modes is dominant during the growth process, NEB calculations were performed with the initial structure being the molecule at a position where the distance between the triple bond atoms and the closest surface atom was at least 4.5 Å and the final structures being the *on-top* and *end-bridge* modes. The resulting energy profiles are given in Figs. 5 and 6.

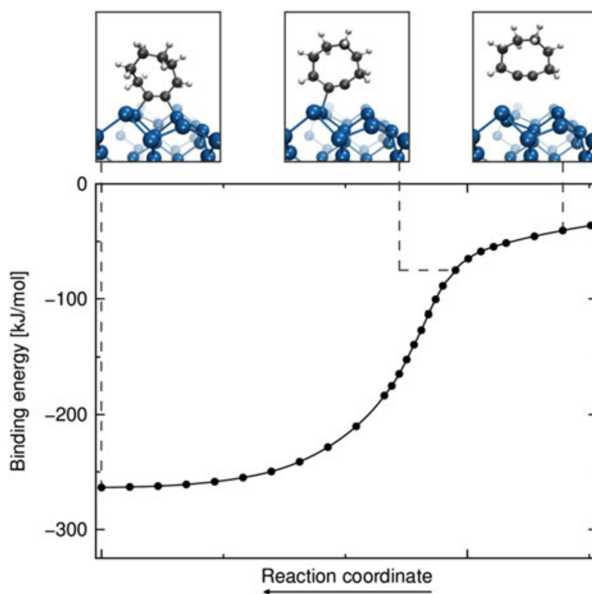

Fig. 6 Energy profile of the *end-bridge* adsorption path with structures shown at selected points. The binding energy is calculated with respect to the isolated and relaxed molecule and surface, respectively

The *on-top* adsorption (Fig. 5) shows a flat plateaux-like shape in the region where the first bond formation takes place (see central top insert), but a local minimum does not emerge and the whole adsorption process does not feature any barrier. A symmetric approach of the triple bond atoms to the lower silicon atom of the dimer reflects the proposed reaction mechanism of ethylene with the Si(001) surface, [23] but that reaction features a local minimum while this one does not. The *end-bridge* adsorption (Fig. 6) also does not feature any local minimum, while in contrast to the *on-top* adsorption, the lower silicon atom is approached in an asymmetric fashion and a plateaux region does not emerge.

Due to both processes being barrierless, the adsorption of the molecule to the surface can not be kinetically controlled. However, adsorption to the *on-top* structure follows a much steeper pathway, making it more likely. Comparison of the final adsorption energies (*On-top*: −306 kJ/mol, *end-bridge*: −263 kJ/mol) should favor the *on-top* mode from a thermodynamical point of view, i.e. if an equilibrium can be reached. This would require a thermally accessible pathway between the two structures, requiring at least one bond to be broken. From the NEB calculations discussed above, where the singly bonded state is about 130 kJ/mol above the minima, it can be estimated that an equilibrium will not be reached at room temperature. For further analysis, *ab-initio* molecular dynamics simulations were carried out.

2.5 Ab-initio Molecular Dynamics Results

Before putting molecule and slab in one simulation, each had to be thermally equilibrated first. For the molecule, 20 simulations at 300 K with 10 ps length were conducted, with the $t=0$ velocities initialized randomly according to a Maxwell-Boltzmann distribution at the given temperature. The slab was initialised in the same way at 300 K, but only one simulation was conducted, where after 10 ps of simulation time, the positions and velocities of the atoms were extracted every 3 ps to yield the 20 starting structures and velocities for further proceedings.

For the actual molecule-surface simulation, the positions and velocities were combined into 20 pairs where in each case the molecule was placed at $\approx$6 Å distance to the surface in z direction and displaced in the x and y directions by adding a random decimal fraction of the cell vector for each using a true random number generator [24]. Thermal translational motion was added to the molecule by again adding random decimal fractions for each velocity component while scaling the length of the vector to the mean Maxwell-Boltzmann velocity of cyclooctyne at 300 K being $\langle v \rangle = 108.18\,\frac{\mathrm{m}}{\mathrm{s}}$ and ensuring that the z component was pointing in the direction of the surface.

Twenty individual simulations were performed and a simulation was considered finished when the molecule was in a clearly bound state and the two C-Si bond lengths had not changed in 500 fs aside from their vibrational motion. Out of these 20 simulations, 17 ended up in the *on-top* state and only 3 in the *end-bridge* state. While 20 simulations do not represent a statistical distribution, the results imply that the *on-top* mode might indeed be the favoured adsorption mode and the predominant reaction in the growth process leading to this semiconductor/organic interface. This is in agreement with the assumption, that the steeper path favours adsorption into the *on-top* mode.

3 Gas Phase Decomposition of MOVPE Precursors: Prelude to Adsorption and Growth Studies

The gas phase decomposition of common MOVPE-precursors has been studied using density functional methods [25–27]. By combining thermodynamic, kinetic and chemical bonding considerations, decomposition pathways and products could be identified. Descriptors based on partial charges were proposed to guide rational design of further precursors. This will be complemented by studies of adsorption and growth on a large scale, employing NEB and MD techniques as described above.

4 GaP/Si-Interfaces in Different Crystal Orientations

Interfaces play an important role in determining the properties of optoelectronic materials. Understanding specific structures, their origin and structure-property relations is thus crucial for material design. In the case of GaP epitaxially grown on Si, intermixing has been observed, leading to the formation of pyramidically shaped patterns [28]. Here, we present energetic considerations evolving around strain and a study of the electrostatic potential across interface regions.

4.1 Strain in Growth Direction

Strain cannot be avoided in the construction of heterostructures and strongly influences the atomic structure and electronic properties of the resulting materials. To study the effects of strain on the lattice matched system GaP/Si, periodic cells with interfaces in (001), (111) and (112) lattice planes have been constructed and are shown in Fig. 7. The thickness of the resulting films varied between 16 and 24 atomic layers, depending on the crystal plane defining the interface.

To enable a meaningful comparison of formation energies for the interfaces, the following definition for the interface formation energy ΔE_{if} has been used:

$$\Delta E_{\mathrm{if}} = \left(N \cdot E_{\mathrm{GaPSi}} - \frac{N}{2} \left(E_{\mathrm{Si}}^{\mathrm{ref}} + E_{\mathrm{GaP}}^{\mathrm{ref}} \right) \right) \cdot A_{(001)}^{-1}. \quad (1)$$

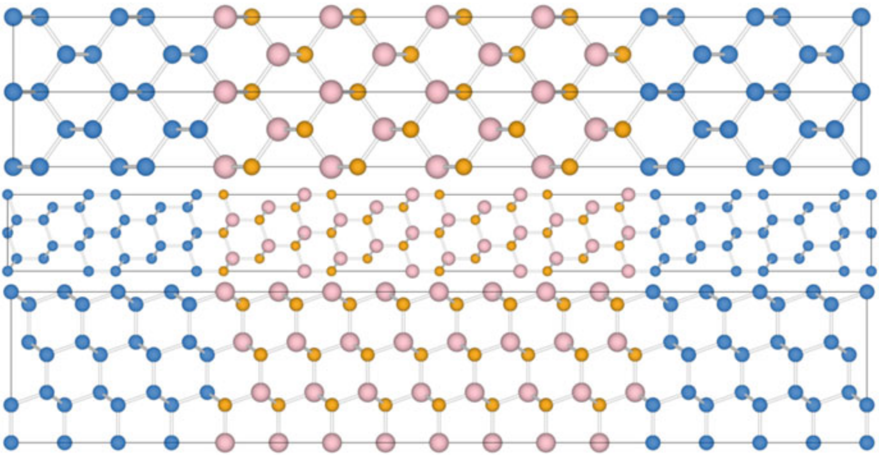

Fig. 7 Supercells used for interface study. From *top to bottom*: (001), (111) and (112) interface. *Blue*: Si, *pink*: Ga, *orange*: P

Here, E_{GaPSi}, $E_{\mathrm{Si}}^{\mathrm{ref}}$ and $E_{\mathrm{GaP}}^{\mathrm{ref}}$ are the total energy of the supercell containing the interface, and a structurally identical reference cell with pure Si and GaP, respectively. The factor $N/2$ with $N = 2$ accounts for the presence of two interfaces in the model cell and the normalization to the interface area for a (001) interface $A_{(001)}$ enables comparison of models with different numbers of atoms.

The interface formation energy as a function of z-axis elongation, where z is the axis perpendicular to the interface plane, is shown in Fig. 8. It is evident that the interface formation energy depends strongly on the crystal plane. The (112) interface is the most stable one, with a formation energy of 0.95 eV per normalization area ($A_{(001)} = 29.5\,\text{Å}^2$) for no z-axis elongation (corresponding to the Si lattice constant). For the (111) interface, the formation energy is slightly higher (1.1 eV), while the (001) interface is the least stable with 1.9 eV. Furthermore, the non-elongated structures represent the actual structure well, as can be seen by the very low energy gain due to elongation in z-direction. It should be noted, that the optimum elongation depends on the interface orientation and is 0.20 % for (111), 0.25 % for (112) and 0.65 % for the (001) orientation. However, the order of interface stabilities remains for elongated cells.

The observations above pose an explanation for the observed formation on intermixing layers at Si/GaP (001) boundaries. Since the (111) and (112) orientations are more stable, their formation is preferred. An important aspect of interface

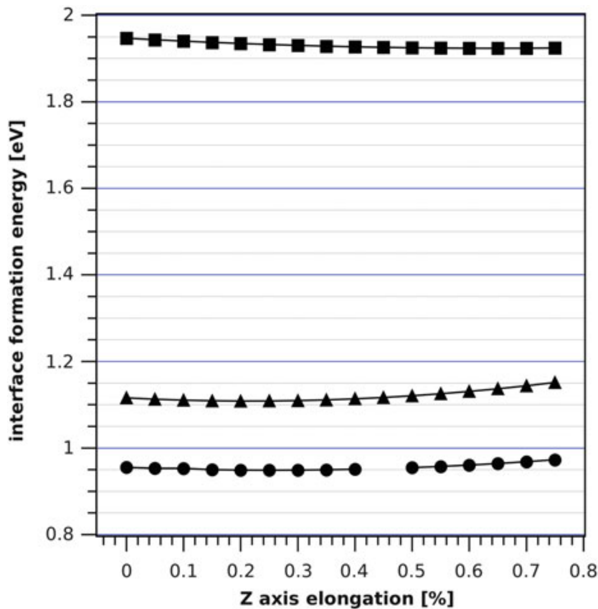

Fig. 8 Interface formation energy according to Eq. (1) for elongated supercells with interfaces in the crystal planes (001) (*squares*), (111) (*triangles*) and (112) (*circles*). Zero elongation corresponds to the experimental lattice constant of Si

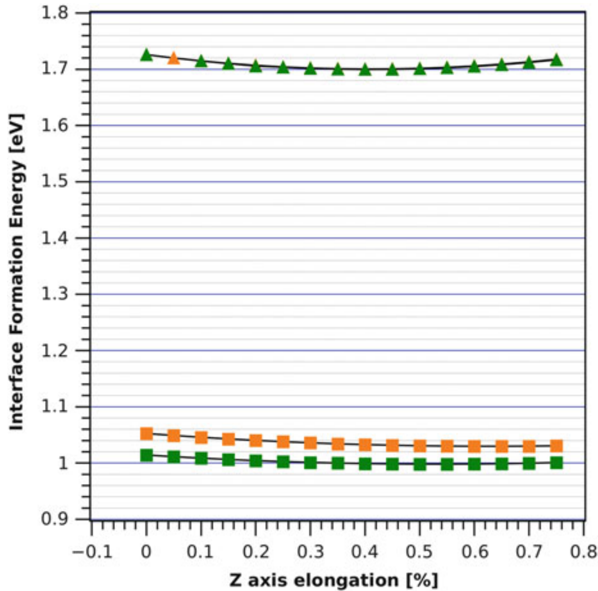

Fig. 9 Interface formation energy according to Eq. (1) for elongated supercells with intermixed interfaces in the crystal planes (001) (*squares*) and (111) (*triangles*). The intermixed atomic layers contain either exclusively Si, Ga (*green*) or Si, P (*orange)* in the intermixing layer. Data point in the (111)-line left out to show that lines coincide

stability is charge neutrality. Ga and P carry different (partial) charges, destabilizing interfaces that lead to charge accumulation. In the case of the (001) and (111) orientation, interfaces are entirely composed of either Ga or P on the GaP side. In the model cells with two interfaces here, each termination occurs once. For the (112) orientation, two mixed terminations dominated by either component is formed. If an intermixed layer is introduced into the (001) and (111) terminations, two identical interfaces in the cell result, either containing Si and Ga or Si and P. As shown in Fig. 9, the introduction of intermixed layers strongly stabilizes the interface formation for the (001) orientation, where intermixing of Si and Ga is slightly more favourable than Si and P. In the case of the (111) interface, intermixing leads to destabilization. The origin of this is the bilayer structure of this interface, which is charge neutral within itself. This internal charge neutrality is broken by intermixing leading to the observed destabilization. The (112) oriented interface is already mixed, making the introduction of one intermixed atomic layer obsolete.

In conclusion, the occurrence of intermixing in the GaP/Si-interface can be explained by the energetic stability of various orientations, which leads to a divergence from a perfectly smooth boundary.

4.2 Electrostatic Potentials Across the GaP/Si-Interface

The performance of a semiconductor device is strongly determined by the electronic structure of its constituents and the interfaces between those. By plotting the plane-averaged local potential in growth direction for the supercells described above, the electrostatic properties and internal dipole moments of the films and interfaces can be studied.

In Fig. 10 the averaged local potential in stacking direction is shown for the (001), (111) and (112) oriented interfaces. In the (001) and (111) interface cells, the local potential oscillates strongly due to the layers consisting of exclusively Ga or P, while in the intrinsically mixed (112) interface cell the oscillations are weaker. A dipole over the film can be recognized for all three cells and can be attributed to either side being dominated (or fully comprised) of one species. A corresponding effect can be seen in the Si to compensate the polarization of the GaP layer. The film dipole is less pronounced for the (112) orientation.

5 Density Functional Computations on the Electronic Structure of Dilute GaAs: Method Validation

The design of optoelectronic devices requires understanding the optical properties of the employed materials. These can be computed by microscopic theories, which build on an accurate description of the electronic bandstructure [29]. The common approach of using interpolated experimental data in the framework of $\mathbf{k} \cdot \mathbf{p}$-theory can be replaced by *ab initio* bandstructure calculations, sufficient accuracy provided.

The systems of interest are multinary III/V-semiconductors, in general dilute GaAs. Thus, simple GaAs is a reasonable choice for method calibration. By comparing a GGA, a hybrid and a meta-GGA functional, namely PBE, HSE06 and TB09 (MBJLDA), respectively, the latter has been chosen for further work, as it yields accurate results for a reasonable computational cost (in agreement with [30]). This allows the use of large supercells for the dilute compounds, enabling the study of the effect structural changes, e.g. the distribution of impurities, have on the electronic structure. From the unfolded supercell bandstructure, as is shown in Fig. 11 for a simple GaAs supercell, the input parameters for the $\mathbf{k} \cdot \mathbf{p}$-theory can be extracted. A computational approach allows not only to predict the properties of new materials, thus guiding the development process, but also to study the effect of local structural motifs on the electronic structure.

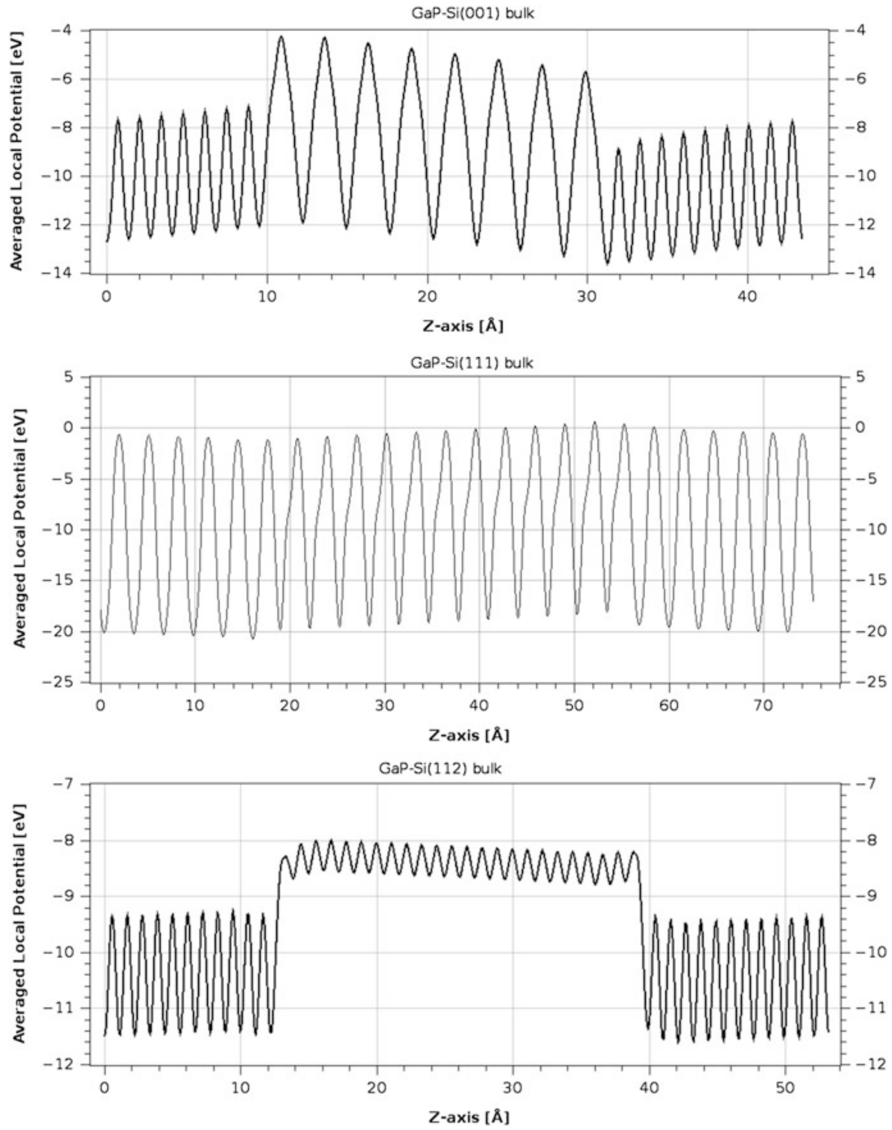

Fig. 10 Plane-averaged local potential along z-direction (perpendicular to interface plane) for (001) (*top*), (111) (*middle*) and (112) (*bottom*) interfacial plane

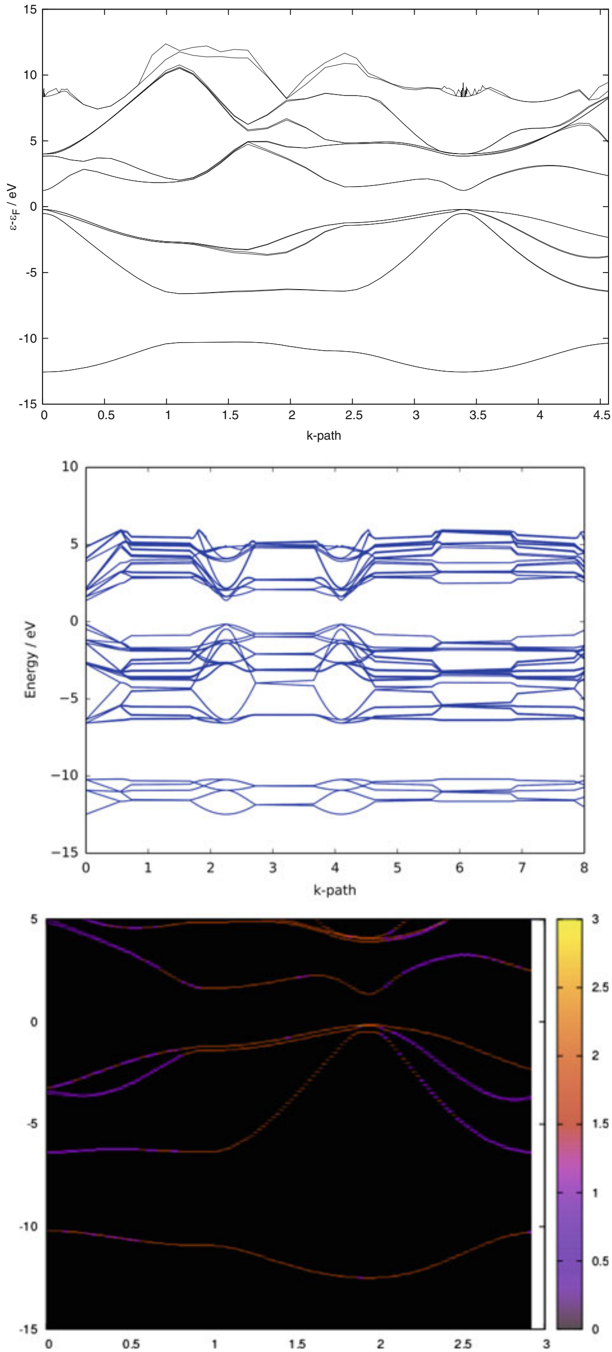

Fig. 11 Bandstructure of GaAs in (*top*) a primitive cell, (*middle*) a 2×2×2 supercell and (*bottom*) the unfolded bandstructure of the supercell

Table 1 Scaling data on Hornet for a Si slab containing 1280 atoms

	Optimized		Non-optimized	
No. of cores	NCORE	t_{eff}/Ms	NCORE	t_{eff}/Ms
528	24	14.95	—	—
2064	48	11.84	24	18.74
4104	57	16.77	24	25.25

The effective time t_{eff} is the elapsed time times the number of cores

6 Scaling Tests

Some scaling tests have been performed on the Hornet cluster in order to control optimal settings for the setting NCORE. This variable is complementary to NPAR, which was described earlier (see Sect. 2). The product of both yields the number of cores per group defined by KPAR (which was set to one in this test). Two settings have been tested. The first one, henceforth dubbed non-optimized, was obtained by setting NCORE to the number of cores per node, i.e. 24. In the second one (optimized), NCORE was set close to the generally recommended value of the square root of the number of nodes. While only very few data points have already been obtained, the effect of setting NCORE to a proper value is quite impressive, leading to a speed-up of roughly one third (see Table 1). It should also be noted, that increasing the number of cores with non-optimized setting does not lead to a speed-up, but has a negative effect. For the optimized settings, it can be seen that increasing the number of cores with optimized settings leads to a speed up in effective time when going from 528 to 2064 cores. Going to 4104 cores actually deteriorates that. This can probably be attributed to the set value of NCORE being close to the square root of the number of cores but not ideal for the actual workload distribution.

Acknowledgements The authors acknowledge the research training group (Graduiertenkolleg, DFG) 1782 "Functionalization of Semiconductors", the collaborative research centre (Sonderforschungsbereich, DFG) 1083 "Structure and Dynamics of Internal Interfaces" and the Beilstein Institut, Frankfurt am Main, for support.

References

1. Mette, G., Dürr, M., Bartholomäus, R., Koert, U., Höfer, U.: Real-space adsorption studies of cyclooctyne on Si(001). Chem. Phys. Lett. **556**, 70 (2013)
2. Schober, C.: Theoretische Untersuchungen der Adsorption von Ethin und Cyclooctin auf der Si(001)-Oberfläche. Master's thesis, Philipps-Universität Marburg (2012)
3. Jónsson, H., Mills, G., Jacobsen, K.W.: In: Berne, B.J., Ciccotti, G., Coker, D.F.: Classical and Quantum Dynamics in Condensed Phase Simulations. World Scientific, Singapore (1998)
4. Hohenberg, P., Kohn, W.: Inhomogeneous electron gas. Phys. Rev. **136**(3B), B864 (1964)
5. Kohn, W., Sham, L.J.: Self-consistent equations including exchange and correlation effects. Phys. Rev. **140**(4A), A1133 (1965)

6. Kresse, G., Furthmüller, J.: Efficiency of ab-initio total energy calculations for metals and semiconductors using a plane-wave basis set. Comp. Mat. Sci. **6**, 15 (1996)
7. Kresse, G., Furthmüller, J.: Efficient iterative schemes for ab initio total-energy calculations using a plane-wave basis set. Phys. Rev. B **54**, 11169 (1996)
8. Perdew, J.P., Burke, K., Ernzerhof, M.: Generalized gradient approximation made simple. Phys. Rev. Lett. **77**, 3865 (1996)
9. Perdew, J.P., Burke, K., Ernzerhof, M.: Erratum: Generalized gradient approximation made simple. Phys. Rev. Lett. **78**, 1396 (1997)
10. Grimme, S.: Density functional theory with London dispersion corrections. WIREs Comput. Mol. Sci. **1**(2), 211 (2011)
11. Grimme, S., Ehrlich, S., Goerigk, L.: Effect of the damping function in dispersion corrected density functional theory. J. Comput. Chem. **32**, 1456 (2011)
12. Blöchl, P.E.: Projector augmented-wave method. Phys. Rev. B **50**, 17953 (1994)
13. Kresse, G., Joubert, D.: From ultrasoft pseudopotentials to the projector augmented-wave method. Phys. Rev. B **59**, 1758 (1999)
14. Monkhorst, H.J., Pack, J.D.: Special points for brillouin-zone integrations. Phys. Rev. B **13**(12), 5188 (1976)
15. Hestenes, M.R., Stiefel, E.: Methods of conjugate gradient for solving linear systems. J. Res. Natl. Bur. Stanf. **49**(6), 409 (1952)
16. Nocedal, E.: Updating quasi-newton matrices with limited storage. Math. Comput. **35**, 773 (1980)
17. Born, M., Oppenheimer, R.: Zur Quantentheorie der Molekeln. Ann. Phys. **84**, 457 (1927)
18. Verlet, R.: Computer "experiments" on classical fluids. i. thermodynamical properties of lennard-jones molecules. Phys. Rev. **159**(1), 98 (1967)
19. Verlet, L.: Computer "experiments" on classical fluids. ii. equilibrium correlation functions. Phys. Rev. **165**(1), 201 (1967)
20. Nose, S.: A unified formulation of the constant temperature molecular dynamics methods. J. Chem. Phys. **81**(1), 511 (1984)
21. Hoover, W.G.: Canonical dynamics: equilibrium phase-space distributions. Phys. Rev. A **31**(3), 1695 (1985)
22. D.J. Evans, B.L. Holian, The nose-hoover thermostat. J. Chem. Phys. **83**(8), 4069 (1985)
23. S.F. Bent, Organic functionalization of group IV semiconductor surfaces: principles, examples, applications, and prospects. Surf. Sci. **500**, 879 (2002)
24. Random.org true random number service. URL http://www.random.org/decimal-fractions. Accessed 21.04.2015
25. Stegmüller, A., Rosenow, P., Tonner, R.: A quantum chemical study on gas phase decomposition pathways of triethylgallane (TEG, Ga(C2H5)3) and tert-butylphosphine (TBP, PH2(t-C4H9)) under MOVPE conditions. Phys. Chem. Chem. Phys. **16**(32), 17018 (2014)
26. Stegmüller, A., Tonner, R.: The beta-hydrogen elimination mechanism in absence of acceptor orbitals in $EH_2(t\text{-}C_4H_9)$ (E = N-Bi). Inorg. Chem. **54**(13), 6363 (2015)
27. Stegmüller, A., Tonner, R.: A quantum-chemical descriptor for CVD precursor design: predicting decomposition rates of TBP and TBAs isomers and derivatives. Chem. Vap. Deposition, **21**, 161–165 (2015). doi:10.1002/cvde.201504332
28. Beyer, A., Oelerich, J.O., Jandieri, K., Werner, K., Stolz, W., Baranovskii, S.D.: Tonner, R., Volz, K.: Pyramidal Structure Formation at the Interface between III/V Semiconductors and Silicon (2015, submitted)
29. Koukourakis, N., Buckers, C., Funke, D.A., Gerhardt, N.C., Liebich, S., Chatterjee, S., Lange, C., Zimprich, M., Volz, K., Stolz, W., Kunert, B., Koch, S.W., Hofmann, M.R.: High room-temperature optical gain in ga(nasp)/si heterostructures. Appl. Phys. Lett. **100**, 092107 (2012)
30. Kim, Y.S., Marsman, M., Kresse, G., Tran, F., Blaha, P.: Towards efficient band structure and effective mass calculations for III-V direct band-gap semiconductors. Phys. Rev. B **82**(20), 205212 (2010)